Crystal Structure and Photoluminescence Evolution of La$_5$(Si$_{2+x}$B$_{1-x}$)(O$_{13-x}$N$_x$):Ce^{3+} Solid Solution Phosphors

Zhiguo Xia,*,† Maxim S. Molokeev,‡,§ Won Bin Im,*,∥ Sanjith Unithrattil,∥ and Quanlin Liu†

†School of Materials Sciences and Engineering, University of Science and Technology Beijing, Beijing 100083, China
‡Laboratory of Crystal Physics, Kirensky Institute of Physics, SB RAS, Krasnoyarsk 660036, Russia
§Far Eastern State Transport University, Serysheva str. 47, Khabarovsk 680021, Russia
∥School of Materials Science and Engineering, Chonnam National University, 300, Yongbong-dong, Buk-gu, Gwangju 500-757, South Korea

Ⓢ Supporting Information

ABSTRACT: A series of iso-structural La$_5$(Si$_{2+x}$B$_{1-x}$)(O$_{13-x}$N$_x$):Ce^{3+} phosphors with apatite structure have been prepared. A combination of powder X-ray diffraction and neutron scattering technique was employed to explore the crystal structural evolution and the rigid nature from oxy- to oxynitride-based apatites, and some local structures were also characterized by HRTEM and ^{29}Si NMR data, respectively. The new La$_5$(Si$_{2+x}$B$_{1-x}$)(O$_{13-x}$N$_x$):Ce^{3+} solid solution phosphors gave continuously controlled emission from 421 nm [La$_5$Si$_2$BO$_{13}$:Ce^{3+}, end-member (x = 0)] to 463 nm (La$_5$Si$_3$O$_{12}$N:Ce^{3+}, end-member (x = 1)). Substitution of B^{3+} and O^{2-} by Si^{4+} and N^{3-} in La$_5$(Si$_{2+x}$B$_{1-x}$)(O$_{13-x}$N$_x$):Ce^{3+} phosphors produced more covalency into the crystal field environment around the Ce^{3+} ions inducing the red-shifted emission, further improving the thermal stability of the oxynitride-based apatite phosphors. The proposed approach from oxy- to oxynitride based iso-structural phases could significantly contribute to future research in designing complex solid solution phosphors.
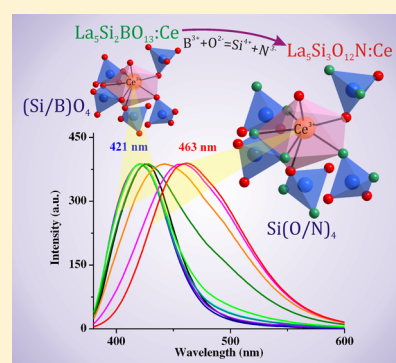
1. INTRODUCTION

As a classical family of luminescence materials host, apatite-type compounds have drawn much attention owing to their adjustable chemical compositions in isostructural compounds with stable physical and chemical properties.[1−5] As it is well-known, the apatite structure belongs to the hexagonal symmetric system with a general chemical formula of the form A$_{10}$(XO$_4$)$_6$Z$_2$ (A = Ca^{2+}, Ba^{2+}, Ce^{3+}, La^{3+}, Y^{3+}, etc., X = P^{5+}, As^{5+}, Si^{4+}, etc., and Z = O^{2-}, F$^-$, Cl$^-$, OH$^-$, etc.).[6−10] For the A$_{10}$[PO$_4$]$_6$Z$_2$ compound, there are two kinds of cationic crystallographic sites labeled as A(I) and A(II) with the local symmetry C_3 and C_s, respectively. Therefore, it is interesting and significant to study the apatite compounds which possess the capability of substitution by other versatile ions and form solid solution. Among them, La$_5$Si$_2$BO$_{13}$ is iso-structural with natural fluoroapatite Ca$_{10}$(PO$_4$)$_6$F$_2$, which crystallizes in the hexagonal symmetric system with the space group of $P6_3/m$.[11,12] In former, both Si and B atoms are located on the tetrahedral site as a member of [SiO$_4$]$^{4-}$ and [BO$_4$]$^{5-}$ tetrahedra. The two kinds of cationic crystallographic sites labeled as La(I), which locates in the general 4f Wyckoff sites with C_3 point symmetry, and the other as La(II), which is the 7-fold coordinated 6h site with C_s point symmetry. The average La−O distances corresponding to these two sites are 2.61 and 2.52 Å, respectively.[12] La$_5$Si$_3$O$_{12}$N also belongs to the hexagonal system with the space group $P6_3/m$ (no. 176),

irrespective of the replacement of B^{3+}−O^{2-} by the Si^{4+}−N^{3-} group.[13] Therefore, based on an appropriate choice of anions and cations, many iso-structural compounds can be realized in some apatite-type compounds. Accordingly, we can fabricate some new phosphors depending on different chemical compositions for the applications in the fields of illumination and display, such as solid state lighting based on the phosphor-converted white light emitting diodes.

Recently, the study on solid solution phosphors has received plenty of attention. In the course of the present investigation, La$_5$(Si$_{2+x}$B$_{1-x}$)(O$_{13-x}$N$_x$) solid solution compounds based on the combination of the La$_5$Si$_2$BO$_{13}$ (oxy-apatite) and La$_5$Si$_3$O$_{12}$N (oxynitride−apatite) phases have been prepared by substituting the coupled B^{3+}−O^{2-} by Si^{4+}−N^{3-}. The structure of oxy-apatite consists of [SiO$_4$] tetrahedra, which can be partially replaced by [Si[O/N]$_4$] tetrahedra. The [SiO$_4$] or [Si[O/N]$_4$] units are stacked together by sharing their corners or edges through O^{2-} ions to form a condensed framework. In the formation of solid-solution, replacing ion pairs, B^{3+} and O^{2-} by Si^{4+} and N^{3-}, modifies electrostatic properties that influence the spectroscopic properties and

luminescence dynamics of the doped Ce^{3+} optical centers but keeps the iso-structure and stability of the crystalline lattice.

Previously, $La_5Si_2BO_{13}$:Ce^{3+} phosphor was reported as a kind of violet-blue emitting phosphor,[14] and $La_5Si_3O_{12}N$:Ce^{3+} gave blue emission.[13] However, the structural association and the phase evolution of these two iso-structural apatite phases, and the investigations on photoluminescence properties in $La_5(Si_{2+x}B_{1-x})(O_{13-x}N_x)$:$Ce^{3+}$ solid solution phosphors, have not been reported until now. This study not only sheds light on the exploration of potential novel phosphors for the practical applications but also reveals the correlations between local structure and luminescence properties of rare earth ion-doped inorganic materials. Therefore, the as-obtained solid-solution phosphors can be used as the blue-component in the fabrication of near-UV pumped light emitting diodes (LEDs). Since the emission peaks can be controlled by the chemical compositions, and the thermal stability can be enhanced with the introduction of nitrogen elements, this new strategy on the design of the solid solution phosphors and the as-obtained phosphors will be very important for the foundation research on phosphors and the related potential applications.

2. EXPERIMENTAL PROCEDURE

$La_5(Si_{2+x}B_{1-x})(O_{13-x}N_x)$:$Ce^{3+}$ (x = 0, 0.1, 0.2, 0.3, 0.4, 0.5, 0.6, 0.7, 0.8, 0.9, and 1.0) phosphors were synthesized by the traditional high-temperature solid-state method from stoichiometric mixtures of the raw materials SiO_2 (A.R.), B_2O_3 (A.R.), Si_4N_3(99.99%), La_2O_3 (99.99%), and CeO_2 (99.99%). The precursors were thoroughly mixed by grinding in an agate mortar, and the final mixture was placed in an alumina crucible and was annealed at 1400−1500 °C, depending on different chemical compositions in a reducing (5% H_2 + 95% N_2) atmosphere for 5 h. After that, the samples were furnace-cooled to room temperature and ground into powder for further analysis.

The phase structure of as-prepared samples were checked through the X-ray powder diffractometer (XRD-6000, SHIMADZU, Japan) using Cu Kα radiation (λ = 0.15406 nm) operated at 40 kV and 30 mA. Neutron power diffraction (NPD) data of the selected samples $La_5(Si_{2+x}B_{1-x})(O_{(13-x)}N_x)$ with x = 0, 0.7, and 1 for Rietveld analysis were collected at room temperature using a high resolution power diffractometer at the Hanaro Center of Korea Atomic Energy Research Institute. The NPD data were collected over a scanning range of $10.5° \leq 2\theta \leq 160°$ with a step size of 0.05° using a neutron beam of wavelength 1.83515 Å. Rietveld refinement was performed by using TOPAS 4.2.[15] ^{29}Si solid-state nuclear magnetic resonance (NMR) experiments were performed on an 80 MHz solid-state Avance Bruker NMR. High-resolution transmission electron microscope (HRTEM) images were checked by a JEOL JEM-2010 microscope with an accelerated voltage of 200 kV. Photoluminescence excitation (PLE) and emission (PL) spectra were performed by using a fluorescence spectrophotometer (F-4600, HITACHI, Japan) equipped with a photomultiplier tube operating at 500 V and a 150 W Xe lamp used as the excitation lamp. The temperature-dependent luminescence properties were measured on the same spectrophotometer, which was equipped with a homemade heating cell and a computer-controlled electric furnace (Tianjin Orient KOJI Co., Ltd., TAP-02). The internal quantum efficiency was measured by using the integrating sphere on the Edinburgh instrument FLSP920 fluorescence spectrophotometer.

3. RESULTS AND DISCUSSION

The phase purity of the as-prepared samples was first checked by XRD patterns. Figure 1a shows the XRD patterns of
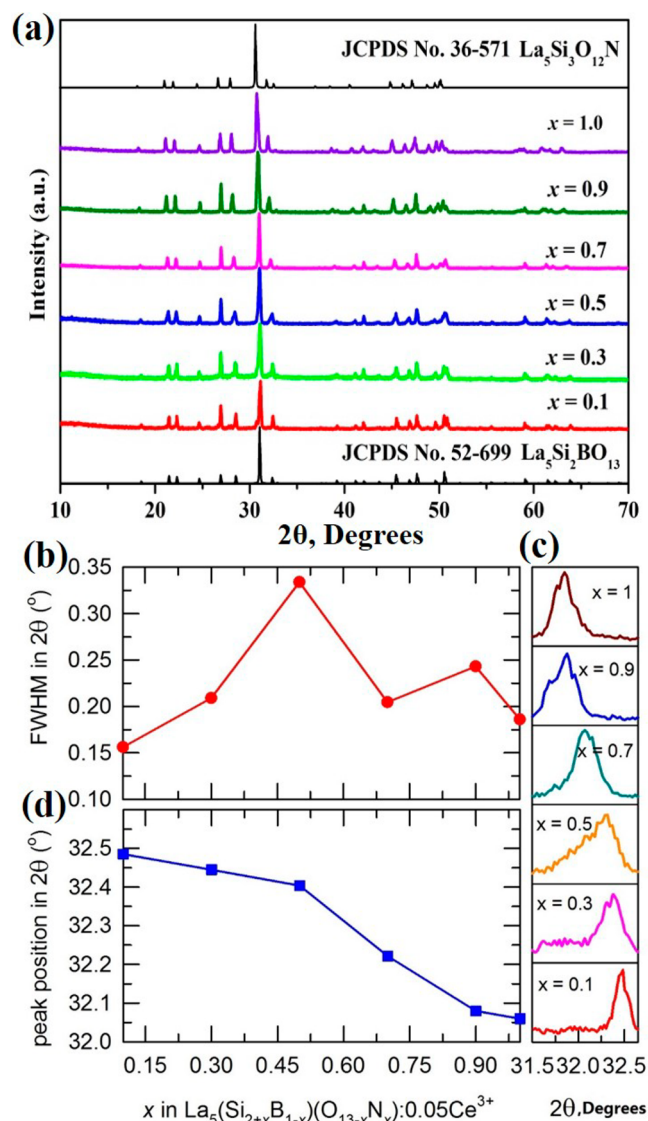
Figure 1. (a) XRD patterns of $La_5(Si_{2+x}B_{1-x})(O_{13-x}N_x)$ (x = 0.1, 0.3, 0.5, 0.7, 0.9, and 1.0), and the standard data for $La_5Si_2BO_{13}$ (JCPDS card no. 52−699) and $La_5Si_3O_{12}N$ (JCPDS card no. 36−571) are shown as a comparison. (b) Variation in fwhm of diffraction peak corresponding to (300) plane with increase of x, (c) the magnified view of the diffraction peaks of compositional series in the region around $2\theta = 32°$, and (d) variation in diffraction peak position with increase of x.

$La_5(Si_{2+x}B_{1-x})(O_{13-x}N_x)$ (x = 0.1, 0.3, 0.5, 0.7, 0.9, and 1.0), which are consistent with the standard data for $La_5Si_2BO_{13}$ (JCPDS card no. 52-699) and $La_5Si_3O_{12}N$ (JCPDS card no. 36-571). The XRD patterns of the $La_5(Si_{2+x}B_{1-x})(O_{13-x}N_x)$ solid solution can be well-identified as the single-phase patterns, which indicate that $La_5Si_2BO_{13}$ and $La_5Si_3O_{12}N$ compound could form continuous solid solution, and all peaks of all patterns were indexed by hexagonal cell ($P6_3/m$) with parameters close to $La_5Si_2BO_{13}$ or $La_5Si_3O_{12}N$ (apatite-type structures). Diffraction peak position and shape are sensitive to the lattice disorder created by the progressive substitution of

the Si/N in place of B/O. In order to further investigate the variation of the local structure, such as the possibility of lattice disorder, we have analyzed XRD diffraction peaks at relevant Bragg position. As shown in Figure 1 (panels b and c), we can find the broadening of the full width at half-maximum (fwhm) for the diffraction peaks along with the shift of diffraction peak indexed as (300) plane at around 32° with increasing content of Si/N in place of B/O, which indicates lattice disordering on partially introducing Si/N for B/O. Moreover, such a variation of the peak positions can be clearly found to shift to the lower 2θ value (Figure 1d).

However, X-ray diffraction was not able to effectively distinguish the O and N sites because of their similar X-ray scattering factors if we wonder more detailed information on the coordination environment. Rietveld refinement by using neutron powder diffraction (NPD) was performed, and the distribution of O and N atoms in $La_5(Si_{2+x}B_{1-x})(O_{13-x}N_x)$ was clearly determined. The crystal structure of $La_5Si_3O_{12}N$ was taken as the starting model for NPD Rietveld refinement, and the phase purity and site occupancy of the solid solution phosphors at each selected composition corresponding to $x = 0$, 0.7, and 1 were estimated. The observed, calculated, and difference results for the Rietveld refinement neutron patterns, the final refined residual factors and refined structural parameters are summarized in Figure 2 and Table 1. All the refined crystallographic parameters well satisfy the reflection conditions, and good fits were obtained with $\chi^2 = 2.31$, 3.12, and 3.48 for $La_5(Si_2B)O_{13}$ ($x = 0$), $La_5(Si_{2.7}B_{0.3})(O_{12.3}N_{0.7})$ ($x = 0.7$), and $La_5Si_3(O_{12}N)$ ($x = 1$), respectively. The fractional atomic coordinates, isotropic displacement parameters ($Å^2$), and the main bond lengths (Å) for $La_5(Si_2B)O_{13}$, $La_5(Si_{2.7}B_{0.3})$-$(O_{12.3}N_{0.7})$, and $La_5Si_3(O_{12}N)$ from the Rietveld structure analysis of NPD patterns are listed in Tables S1 and S2 of the Supporting Information. Moreover, the crystallographic information files (CIF) of $La_5(Si_{2.7}B_{0.3})(O_{12.3}N_{0.7})$ were also given in the Supporting Information.

Apatite structure can be generally represented by $M1_2$ $M2_3(XO_4)_3Z$, where M is a divalent or trivalent cation, X is a trivalent, tetravalent, or pentavalent cation, and Z is possibly occupied by monovalent or divalent anions.[11] M1 cation occupying the 4f site is coordinated by nine O/N atoms and M2 cation occupying the 6h site is coordinated with 7 O/N atoms. Herein, $La_5Si_{2.5}B_{0.5}O_{12.3}N_{0.7}$ was selected as the example to study the detailed coordination information. In such a structure, both M1 and M2 are La^{3+} ions, while X at 6h is Si/B atoms. Out of the four distinct O/N sites present in the structure, three are part of the $(Si/B)(O/N)_4$. Its crystal structure consists of two independent La ions and one $(Si/B)(O/N)_4$ tetrahedron. All of the cations can form polyhedra and are linked to each other by nodes or edges as shown in Figure 3. The La1 polyhedron connected with four $(Si/B)(O/N)_4$ tetrahedra by nodes and with one tetrahedron by edge, but the La2 polyhedra linked with three tetrahedra by nodes and three tetrahedra by edges. The symmetries of sites of these two La ions are different as the La1 ion is located on mirror plane m, but La2 is on 3-fold axis 3. The La1 and La2 ions in the compound with $x = 0$ are coordinated by seven and nine O^{2-} anions, respectively. The La1O7 has the form of a pentagonal bipyramid (Figure 3b), while La2O9 forms a three-capped trigonal prism (Figure 3c). The compounds with $x = 0.7$ and 1.0 have the same coordination number of La and Si/B ions: CN(La1) = 7; CN (La2) = 9; CN(Si/B) = 4 and the same form of polyhedra, but different ligands, as one O^{2-} anion in
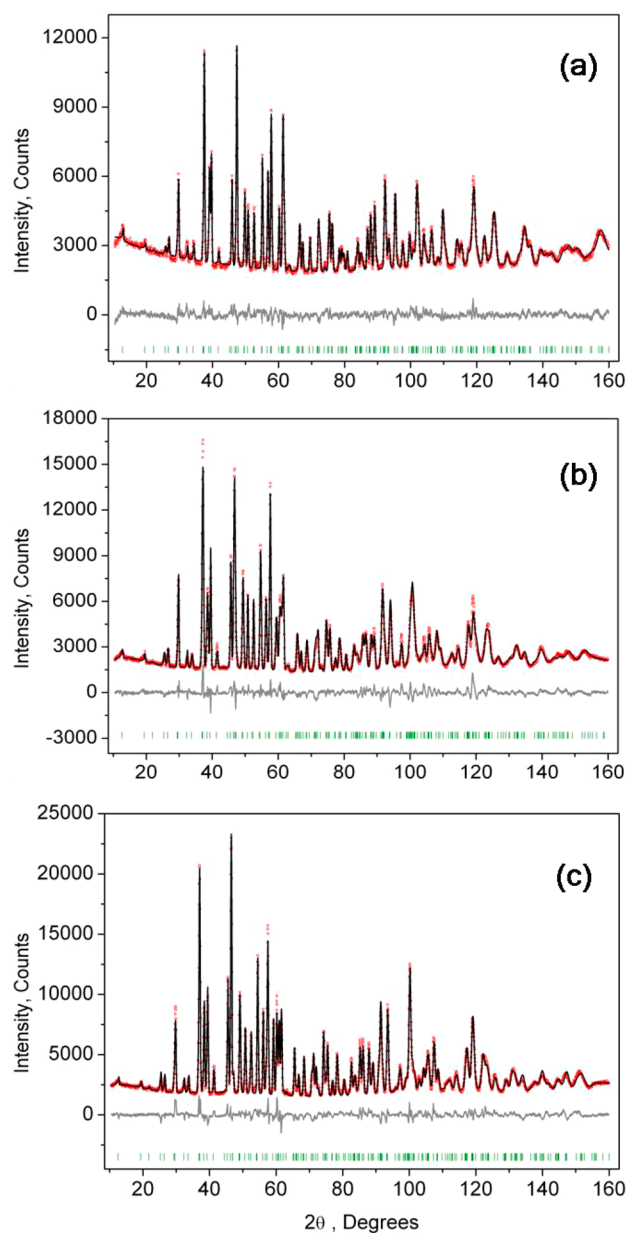
Figure 2. Observed (red crosses) and calculated (black lines) NPD patterns as well as difference profiles (gray lines) and the corresponding Bragg positions (green bars) for Rietveld structure analysis of $La_5(Si_2B)O_{13}$ (a), $La_5(Si_{2.7}B_{0.3})(O_{12.3}N_{0.7})$ (b) and $La_5Si_3(O_{12}N)$ (c).

these compounds are substituted by the N^{3-} anion. The distribution of N on these sites would be such that the bond valence sum (BVS) of the La1 and La2 at M1 and M2 sites, respectively, matches the formal valence. Therefore, the predicted and calculated bond valences of atoms at different sites of $La_5Si_{2.7}B_{0.3}O_{12.3}N_{0.7}$ are listed in Table 2. The primary refinement of neutron diffraction data has shown the bond valence sum (BVS) of 2.93 and 2.98 for La1 and La2, respectively, in place of the formal value, 3. The BVS values of the O/N sites have shown a bond valence of 2.29, 2.21, 2.17, and 2.15, respectively, for O1, O2, O3, and O4 sites instead of the formal value of 2 for the former three and 2.26 for the O4. These indicate an imbalance in assignment of N at a particular site, and instead, a joint O/N site seems to be preferred as these two anions O^{2-} and N^{3-} are not ordered and form one joint O/

Table 1. Main Parameters of Processing and Refinement of $La_5(Si_2B)O_{13}$, $La_5(Si_{2.7}B_{0.3})(O_{12.3}N_{0.7})$, and $La_5Si_3(O_{12}N)$ from the Rietveld Structure Analysis of NPD Patterns

compound	$La_5(Si_2B)O_{13}$ $x = 0$	$La_5(Si_{2.7}B_{0.3})$ $(O_{12.3}N_{0.7})$ $x = 0.7$	$La_5Si_3(O_{12}N)$ $x = 1$
Sp. Gr.	$P6_3/m$	$P6_3/m$	$P6_3/m$
a (Å)	9.5530(2)	9.6658(3)	9.7121(2)
c (Å)	7.2143(2)	7.1900(3)	7.1894(2)
V (Å^3)	570.17(4)	581.75(5)	587.29(3)
Z	2	2	2
2θ range (deg)	10.5−160	10.5−160	10.5−160
no. of reflections	274	279	282
no. of refined parameters	45	47	47
R_{wp} (%)	4.30	5.98	6.15
R_p (%)	3.36	4.62	4.71
R_{exp} (%)	1.86	1.92	1.77
χ^2	2.31	3.12	3.48
R_B (%)	1.98	3.10	3.45
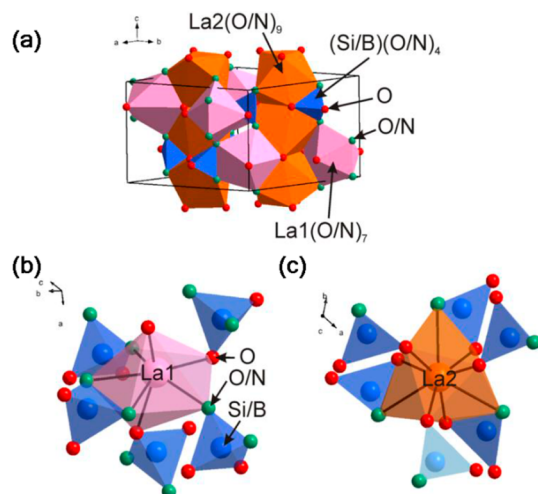
Figure 3. (a) Crystal structure of $La_5(Si_{2+x}B_{1-x})(O_{13-x}N_x)$. The coordination sphere of (b) La1 ion and (c) La2 ion.

Table 2. Predicted and Calculated Bond Valence of Atoms at Different Sites of $La_5Si_{2.7}B_{0.3}O_{12.3}N_{0.7}$

atomic sites	predicted	calculated
La1	3	2.93
La2	3	2.98
Si/B	3.9	4.36
O1	−2.0	−2.29
O2	−2.0	−2.21
O3	−2.0	−2.17
O4/N4	−2.26	−2.01

N site (Table S1 of the Supporting Information). The neutron diffraction pattern proves this disordering because there are no superstructure peaks and peak splitting on the pattern.[16,17]

The compound with $x = 0.7$ differs from the compound with $x = 1.0$ only by proportion of N^{3-} and O^{2-} ions in this O/N site. Therefore, in both compounds with $x = 0.7$ and 1.0 the La1 is coordinated by three O^{2-} and four O/N ions, the La2 is coordinated by six O^{2-} and three O/N ions and Si/B by two O^{2-} and two O/N ions (Figure 3). Since the concentration of B ions decreases with x value and the concentration of N ions increases with x, the cell volume should increase with x because

of ionic radii (IR), (B^{3+}, CN = 4) = 0.11 Å, IR(Si^{4+}, CN = 4) = 0.26 Å and IR (O^{2-}, CN = 4) = 1.38 Å, IR (N^{3-}, CN = 4) = 1.46 Å. As a further examination of the substitution of Si^{4+}/N^{3-} and B^{3+}/O^{2-}, the unit cell parameters (a, c, and V) of solid solutions series obtained from XRD data are shown in Figure 4.
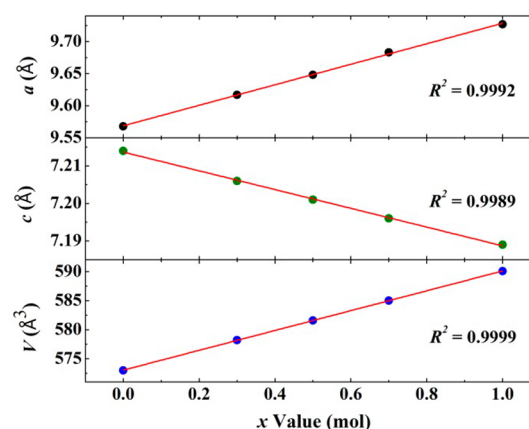
Figure 4. Variation of unit cell parameters (a, c, and V) of $La_5(Si_{2+x}B_{1-x})(O_{13-x}N_x)$ solid-solution series dependent on x values.

It is obvious that the lattice parameter a, c values and cell volume V are proportional to the x value, indicating that the solid solution are iso-structural and also suggest the correctness of chemical formula of compounds, as similar results were reported on the $CaMgSi_2O_6$–$NaScSi_2O_6$ solid solution system.[18]

The fine local structures of $La_5(Si_{2+x}B_{1-x})(O_{13-x}N_x)$ ($x = 0$, 0.7, and 1.0) were also studied by HRTEM technique and fast Fourier transform (FFT) images shown in Figure 5. It is found in Figure 5 (panels b and f) that the lattice fringes with a d spacing of 0.238 and 0.365 nm could be assigned to the (220) and (002) planes with conventional d spacing of 0.239 nm for $La_5Si_2BO_{13}$ and 0.363 nm for $La_5Si_3O_{12}N$, respectively. The lattice fringes have changed slightly owing to the increase of the cell volume with the substitution of Si^{4+}/N^{3-} for B^{3+}/O^{2-} ions. The results further confirm the highly crystalline nature of the composition. To understand the structural evolution in solid solution $La_5(Si_{2+x}B_{1-x})(O_{13-x}N_x)$, d spacing of the principal planes (210) and (002) were calculated and illustrated in Figure 5. The calculated values are 0.312 nm for (210) planes and 0.362 nm corresponding to (002) for the compound with $x = 0.7$. According to the report by Mazza, the d spacing of the principal planes is 0.3607 nm, corresponding to the (002) plane and was identified that the linear structural evolution of d-spacing in the (002) planes could be built as a function of x values in the $La_5(Si_{2+x}B_{1-x})(O_{13-x}N_x)$ series.[11] Furthermore, since the solid-state NMR is sensitive to the local order of nuclei, ^{29}Si NMR analysis was performed to gain insight into the network ordering of $La_5(Si_{2+x}B_{1-x})(O_{13-x}N_x)$ solid solution. Figure 6 shows the ^{29}Si NMR spectra for as-prepared $La_5(Si_{2+x}B_{1-x})(O_{13-x}N_x)$ ($x = 0$, 0.5, 0.7, and 1.0). The isotropic chemical shift in the NMR spectrum is mainly affected by the coordination number of the cation. As shown in Figure 6, a strong contribution at about −78.02 ppm for all of the $La_5(Si_{2+x}B_{1-x})(O_{13-x}N_x)$ solid solution suggests that the structural environment of Si in this series of compounds is nearly the same.[19] As we know, the ^{29}Si NMR spectroscopy provides direct information through the number of peaks and the chemical shifts to reveal the change in structure. A slight
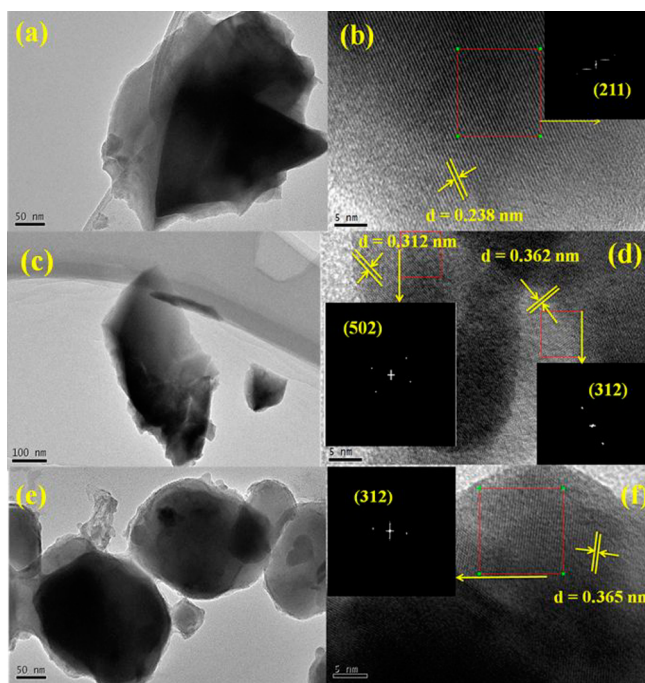
Figure 5. (a) TEM image, (b) HRTEM images of $La_5Si_2BO_{13}$; (c) TEM image, (d) HRTEM images of $La_5(Si_{2.7}B_{0.3})(O_{12.3}N_{0.7})$; (e) TEM image, (f) HRTEM images of $La_5Si_3O_{12}N$; inset in (b, d, and f) shows the fast Fourier transforms (FFTs) of the relevant HRTEM images.
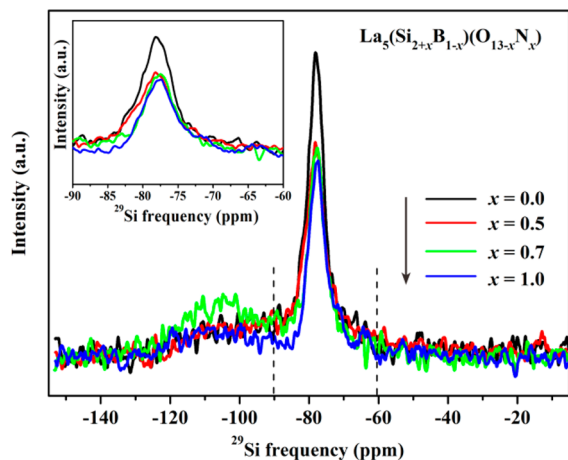
Figure 6. ^{29}Si NMR spectra of as-prepared samples $La_5(Si_{2+x}B_{1-x})$-$(O_{13-x}N_x)$ (x = 0, 0.5, 0.7, and 1.0).

chemical shift showed in the inset of Figure 6, indicates that, with increase in substitution of Si^{4+}/N^{3-} to B^{3+}/O^{2-} ions, the surrounding ^{29}Si nuclei chemical environment changes owing to the Si^{4+}/N^{3-} to B^{3+}/O^{2-} ions replacement.

Though the designed solid solution compounds possess the same apatite structure, various chemical compositions will produce different crystal field environment for the doped activators, which further affects the luminescence properties of the as-prepared solid solution phosphors. In the present case, by the progressive replacement of B^{3+} and O^{2-} with Si^{4+} and N^{3-}, it was expected to introduce more covalency, affecting the crystal field environment around the doped Ce^{3+} ions, and thus the color-tunable emission can be controlled through the change in chemical compositions of the solid solution.[20−22]

The photoluminescence excitation (PLE) spectra of $La_5Si_2BO_{13}:0.05Ce^{3+}$ and $La_5Si_3O_{12}N:0.05Ce^{3+}$ are demonstrated in Figure 7a. The PLE spectrum monitored at 421 and 465
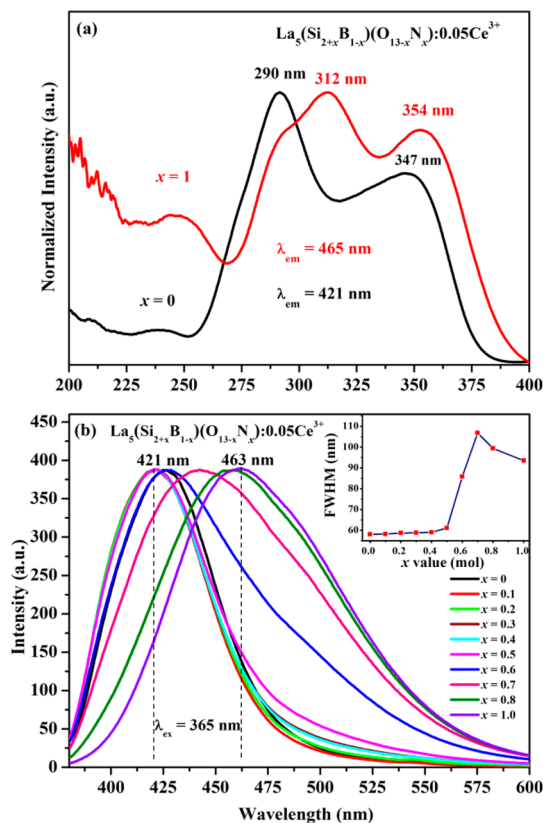
Figure 7. Normalized (a) excitation and (b) emission spectra of $La_5(Si_{2+x}B_{1-x})(O_{13-x}N_x):0.05Ce^{3+}$ (x = 0−1) phosphors under 365 nm UV light excitation. Inset of (b) shows the variation of the fwhm, depending on the x value.

nm exhibit two distinct excitation bands at 290, 347 nm and 312, 354 nm, respectively, which could be ascribed to the electronic transitions from the ground state to the different crystal field splitting bands of excited 5d states of Ce^{3+}. As we know, the excited state $5d^1$ of Ce^{3+} is sensitive to structure changes, and it is essential to understand the preferred crystallographic position for Ce^{3+} occupation. The present apatite structure has two possible sites for Ce^{3+} substitution, which are crystallographically distinct with seven and nine coordination; however, the lack of distinct bands in the emission spectra indicate that dopant ions are selectively occupied at one of the possible sites. The emission peak position of Ce^{3+} has strong dependence on its local environment and therefore an empirical relation proposed by Van Uitert can be used to identify the exact Ce^{3+} substitutional site, and the equation is given below,[23]

$$E\ (cm^{-1}) = Q\left[1 - \left(\frac{V}{4}\right)^{1/V} \times 10^{-(nE_a r)/80}\right] \tag{1}$$

where E is the position for the Ce^{3+} emission peak, Q is the position in energy for the lower d-band edge for the free Ce^{3+} ion (Q = 50000 cm^{-1}), V is the valence of the Ce^{3+} ion (V = 3), n is the number of anions in the immediate shell about the Ce^{3+} ion, E_a is the electron affinity of anion atom in electronvolts, and r is the radius of the host cation replaced by the Ce^{3+} ion

(Å). Here r, the radius of ions, were taken as 1.10 and 1.21 Å for seven- and nine-coordinated La^{3+} ions, respectively, while E_a the electron affinity of both the coordination environment were taken as 1.89 eV. The calculated value of emission peak position of Ce^{3+} substituted at seven-coordinated La1 site with C_s symmetry and nine-coordinated La2 site with C_3 symmetry are 20118 (497 nm) and 24878 cm^{-1} (402 nm), respectively. The calculated emission peak position at 402 nm is closer to the measured emission peak at around 422 nm and is assigned as emission form Ce^{3+} substituted at La2 sites. On the other hand, the measured emission spectra do not have emission bands centered near 497 nm and can be concluded that the Ce^{3+} preferentially occupies the nine coordinated La2 sites in the structure. In addition, it is clearly observed that the excitation peak appears to be red-shifted with the replacement of B^{3+} and O^{2-} by Si^{4+} and N^{3-} because of the stronger covalency.

The normalized emission spectra of $La_5(Si_{2+x}B_{1-x})$-$(O_{13-x}N_x):0.05Ce^{3+}$ ($x = 0-1$) phosphors under 365 nm UV light excitation are shown in Figure 7b. The activator concentration of Ce^{3+} was fixed at 0.05, and the composition of x in the solid solution was varied from 0 to 1. The emission spectra of the samples exhibit a broad nonsymmetrical band, which corresponds to the transitions of the 5d–4f of Ce^{3+} ions. When x value is 0, it forms $La_5Si_2BO_{13}:0.05Ce^{3+}$ phosphor, which was previously reported, with its emission spectra showing a broad band with a peak cantered at about 421 nm. With increasing x value, the emission peak shows an obvious red shift, eventually to 463 nm when x increases to 1. The corresponding variation of CIE chromaticity coordinates (x, y) with different x value, and the digital photos of the samples under a 365 nm UV lamp are demonstrated and summarized in Figure 8. As shown in Figure 8, the color tone can be adjusted from violet (0.159, 0.036) to blue (0.151, 0.173) in the $La_5(Si_{2+x}B_{1-x})(O_{13-x}N_x):Ce^{3+}$ phosphors by varying the chemical composition of the solid solution phosphor. Addi-
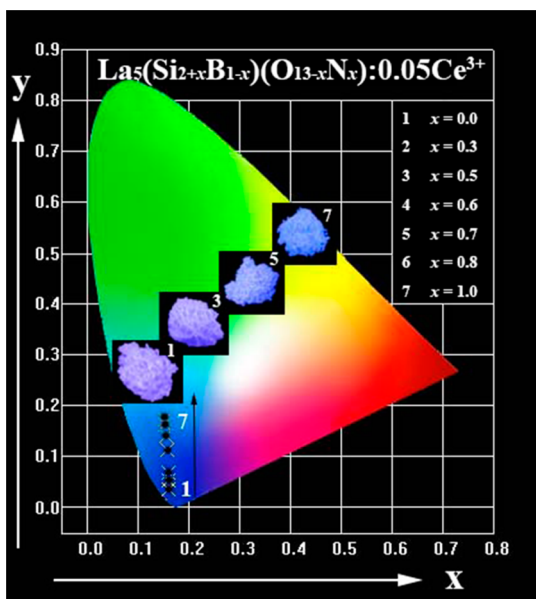
Figure 8. CIE chromaticity coordinates for $La_5(Si_{2+x}B_{1-x})$-$(O_{13-x}N_x):0.05Ce^{3+}$ ($x = 0, 0.3, 0.5, 0.6, 0.7, 0.8$, and 1.0) phosphors upon 365 nm excitation and the digital photos of the selected samples under 365 nm UV lamp excitation.

tionally, the variation of fwhm as a function of x value were shown in the inset of Figure 7. It is clear that the fwhm increases with the increase of x value, and reaches a maximum for $x = 0.7$, and then the fwhm decreases slightly with the increase of x content. The red shift of emission band along with the increase in fwhm of the emission bands could be explained as a combined effect of the lattice disordering and enhanced crystal field strength at emission centers via introducing more covalent N^{3-} ions in place of O^{2-}. The change in crystal field strength is due to the difference in electric charge and the covalence of N^{3-} ions, which are substituted in place of O^{2-}, therefore an increase in the crystal-field strength will split more ground state, such as $^2F_{5/2}$ and $^2F_{7/2}$ energy levels. As also discussed previously, the broadening of fwhm for the diffraction peaks along with the shift of diffraction peaks with increasing content of Si/N in place of B/O can be clearly found. This, in effect, would also have substantial contribution in broadening of the Ce^{3+} emission band.[24]

The thermal stability of phosphor is one of the important undesirable issues to be addressed before recommending for potential applications.[25] Therefore, the temperature-dependent PL properties of the as-prepared $La_5(Si_{2+x}B_{1-x})$-$(O_{13-x}N_x):0.05Ce^{3+}$ ($x = 0, 0.1, 0.3, 0.5$, and 0.7) phosphors were investigated in the temperature range from 30 to 300 °C (Figure 9a). It can be seen that the luminescence intensity of
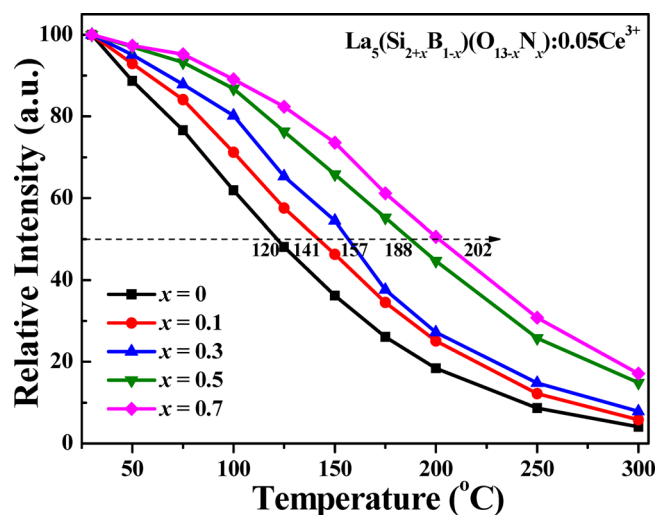
Figure 9. Temperature dependence of the peak emission intensity, normalized to $T = 30$ °C values, for thermal quenching of $La_5(Si_{2+x}B_{1-x})(O_{13-x}N_x):0.05Ce^{3+}$ ($x = 0, 0.1, 0.3, 0.5$, and 0.7) phosphors.

the samples have an obvious decreasing trend with increasing temperature and dropped to 50% of the initial intensity when the temperature was raised up to 120, 141, 157, 188, and 202 °C. It is found that $La_5Si_2BO_{13}:0.05Ce^{3+}$ has a relatively poor thermal stability, however, the thermal stability of this series of $La_5(Si_{2+x}B_{1-x})(O_{13-x}N_x):0.05Ce^{3+}$ gets better with increasing x values. It could be assigned to the exaltation of lattice rigidity and the quenching barrier height caused by progressive replacement of B^{3+} and O^{2-} by Si^{4+} and N^{3-}. On account of above experimental results, it further confirmed that the thermal stability can be successfully improved by the replacement of B^{3+} and O^{2-} by Si^{4+} and N^{3-}. Furthermore, the luminescence internal quantum efficiency of the two end members of $La_5Si_2BO_{13}:0.05Ce^{3+}$ and $La_5Si_3O_{12}N:0.05Ce^{3+}$

were measured and determined to be 29.4% and 22.5%, respectively.[14] However, we can further improve them via the optimization of the experimental procedure and the chemical compositions.

4. CONCLUSIONS

In conclusion, $La_5(Si_{2+x}B_{1-x})(O_{13-x}N_x):Ce^{3+}$ solid solution phosphors have been synthesized via the high-temperature solid-state method. The phase structures determined by the X-ray diffraction and the neutron diffraction Rietveld refinement confirms that the solid solution compounds possess an apatite-type structure via replacement of B^{3+} and O^{2-} by Si^{4+} and N^{3-}. The local structure evolution was also confirmed by the HRTEM examination from the linear variation of d-spacings in the (002) planes with x. The new solid solution phosphors give continuously controlled violet-blue emission and enhanced thermal stability. The red-shift behavior from 421 to 463 nm can be realized with increasing x value in $La_5(Si_{2+x}B_{1-x})$-$(O_{13-x}N_x):Ce^{3+}$. The above results indicate that it is interesting to design color-tunable phosphors on the basis of the control of the chemical compositions of the iso-structural solid solutions phosphors via the crystal chemistry strategy.

■ ASSOCIATED CONTENT

Ⓢ Supporting Information

Fractional atomic coordinates and isotropic displacement parameters ($Å^2$) and the main bond lengths (Å) of $La_5(Si_2B)$-O_{13}, $La_5(Si_{2.7}B_{0.3})(O_{12.3}N_{0.7})$, and $La_5Si_3(O_{12}N)$ from the Rietveld structure analysis of NPD patterns and the crystallographic information files (CIF) of $La_5(Si_{2.7}B_{0.3})(O_{12.3}N_{0.7})$. This Supporting Information associated with this article are presented. This material is available free of charge via the Internet at http://pubs.acs.org.

■ AUTHOR INFORMATION

Corresponding Authors
*E-mail: xiazg@ustb.edu.cn. Tel: +86-10-8237-7955. Fax: +86-10-8237-7955.
*E-mail: imwonbin@chonnam.ac.kr.

Notes
The authors declare no competing financial interest.

■ REFERENCES

(1) Shang, M.; Li, G.; Geng, D.; Yang, D.; Kang, X.; Zhang, Y.; Lian, H.; Lin, J. Blue Emitting $Ca_8La_2(PO_4)_6O_2:Ce^{3+}/Eu^{2+}$ Phosphors with High Color Purity and Brightness for White LED: Soft-Chemical Synthesis, Luminescence, and Energy Transfer Properties. *J. Phys. Chem. C* **2012**, *116*, 10222−10231.

(2) Liu, H.; Luo, Y.; Mao, Z.; Liao, L.; Xia, Z. A Novel Single-Composition Trichromatic White-emitting $Sr_{3.5}Y_{6.5}O_2(PO_4)_{1.5}(SiO_4)_{4.5}:Ce^{3+}/Tb^{3+}/Mn^{2+}$ Phosphor: Synthesis, Luminescent Properties and Applications for White LEDs. *J. Mater. Chem. C* **2014**, *2*, 1619−1627.

(3) Shang, M.; Geng, D.; Yang, D.; Kang, X.; Zhang, Y.; Lin, J. Luminescence and Energy Transfer Properties of $Ca_2Ba_3(PO_4)_3Cl$ and $Ca_2Ba_3(PO_4)_3Cl:A$ (A = $Eu^{2+}/Ce^{3+}/Dy^{3+}/Tb^{3+}$) under UV and Low-Voltage Electron Beam Excitation. *Inorg. Chem.* **2013**, *52*, 3102−3112.

(4) Xie, M.; Tao, Y.; Huang, Y.; Liang, H.; Su, Q. The Quantum Cutting of Tb^{3+} in $Ca_6Ln_2Na_2(PO_4)_6F_2$ (Ln=Gd, La) under VUV−UV Excitation: with and without Gd^{3+}. *Inorg. Chem.* **2010**, *49*, 11317−11324.

(5) Que, M.; Ci, Z.; Wang, Y.; Zhu, G.; Xin, S.; Wang, Q. Crystal Structure and Luminescence Properties of a Cyan Emitting $Ca_{10}(SiO_4)_3(SO_4)_3F_2:Eu^{2+}$ Phosphor. *CrystEngComm* **2013**, *15*, 6389−6394.

(6) Jiao, M. M.; Jia, Y. C.; Lv, W.; Lv, W. Z.; Zhao, Q.; Shao, B. Q.; You, H. P. $Sr_3GdNa(PO_4)_3F:Eu^{2+},Mn^{2+}$: A Potential Color Tunable Phosphor for White LEDs. *J. Mater. Chem. C* **2014**, *2*, 90−97.

(7) Li, K.; Geng, D. L.; Shang, M. M.; Zhang, Y.; Lian, H. Z.; Lin, J. Color-Tunable Luminescence and Energy Transfer Properties of $Ca_9Mg(PO_4)_6F_2:Eu^{2+}$, Mn^{2+} Phosphors for UV-LEDs. *J. Phys. Chem. C* **2014**, *118*, 11026−11034.

(8) Zhou, L.; Liang, H. B.; Tanner, P. A.; Zhang, S.; Hou, D. J.; Liu, C. M.; Tao, Y.; Huang, Y.; Li, L. Luminescence, Cathodoluminescence and $Ce^{3+} \rightarrow Eu^{2+}$ Energy Transfer and Emission Enhancement in the $Sr_5(PO_4)_3Cl:Ce^{3+},Eu^{2+}$ Phosphor. *J. Mater. Chem. C* **2013**, *1*, 7155−7165.

(9) Mi, R. Y.; Zhao, C. L.; Xia, Z. G. Synthesis, Structure and Tunable Luminescence Properties of Novel Ba_3NaLa-$(PO_4)_3F:Eu^{2+},Mn^{2+}$ Phosphors. *J. Am. Ceram. Soc.* **2014**, *97*, 1802−1808.

(10) Zhu, H. K.; Xia, Z. G.; Liu, H. K.; Mi, R. Y.; Hui, Z. Luminescence Properties and Energy Transfer of Bi^{3+}/Eu^{3+}-Codoped $Ca_{10}(PO_4)_6F_2$ Phosphors. *Mater. Res. Bull.* **2013**, *48*, 3513−3517.

(11) Mazza, D.; Tribaudino, M.; Delmastro, A.; Lebech, B. Synthesis and Neutron Diffraction Study of $La_5Si_2BO_{13}$, an Analog of the Apatite Mineral. *J. Solid State Chem.* **2000**, *155*, 389−393.

(12) Yuan, J. L.; Zhang, Z. J.; Wang, X. J.; Chen, H. H.; Zhao, J. T.; Zhang, G. B.; Shi, C. S. Synthesis and VUV−UV Spectroscopic Properties of Rare Earth Borosilicate Oxyapatite: $RE_5Si_2BO_{13}:Ln^{3+}$ (RE=La, Gd, Y; Ln=Eu, Tb). *J. Solid State Chem.* **2007**, *180*, 1365−1371.

(13) Lu, F.; Song, X.; Liu, Q. Crystal Structure and Photo-luminescence of $(La_{1-x}Ce_x)_5Si_3O_{12}N$. *J. Alloys Compd.* **2011**, *509*, 2099−2104.

(14) Liu, H.; Liao, L.; Xia, Z. Structure, Luminescence Property and Energy Transfer Behavior of Color-adjustable $La_5Si_2BO_{13}:Ce^{3+},Mn^{2+}$ Phosphor. *RSC Adv.* **2014**, *4*, 7288−7295.

(15) *TOPAS V4: General Profile and Structure Analysis Software for Powder Diffraction Data User's Manual.* Bruker AXS, Karlsruhe, Germany, 2008.

(16) Shannon, R. D. Revised Effective Ionic Radii and Systematic Studies of Interatomic Distances in Halides and Chalcogenides. *Acta Crystallogr., Sect. A* **1976**, *32*, 751−767.

(17) Brown, I.; Altermatt, D. Bond-Valence Parameters Obtained from a Systematic Analysis of the Inorganic Crystal Structure Database. *Acta Crystallogr., Sect. A* **1985**, *41*, 244−247.

(18) Xia, Z.; Zhang, Y.; Molokeev, M. S.; Atuchin, V. V.; Luo, Y. Linear Structural Evolution Induced Tunable Photoluminescence in Clinopyroxene Solid-solution Phosphors. *Sci. Rep.* **2013**, *3*, 3310-1−3310-7.

(19) Xu, J. G.; Wang, X. M.; Fu, H.; Brown, C. M.; Jing, X. P.; Liao, F. H.; Lu, F. Q.; Li, X. H.; Kuang, X. J.; Wu, M. M. Solid-State ^{29}Si NMR and Neutron-Diffraction Studies of $Sr_{0.7}K_{0.3}SiO_{2.85}$ Oxide Ion Conductors. *Inorg. Chem.* **2014**, *53*, 6962−6968.

(20) Luo, Y.; Xia, Z. G. Effect of Partial Nitridation on the Structure and Luminescence Properties of Melilite-type $Ca_2Al_2SiO_7:Eu^{2+}$ Phosphor. *Opt. Mater.* **2014**, *36*, 1874−1878.

(21) Wu, J. L.; Gundiah, G.; Cheetham, A. K. Structure−Property Correlations in Ce-Doped Garnet Phosphors for Use in Solid State Lighting. *Chem. Phys. Lett.* **2007**, *441*, 250−254.

(22) Geng, D.; Lian, H.; Shang, M.; Zhang, Y.; Lin, J. Oxonitridosilicate $Y_{10}(Si_6O_{22}N_2)O_2$:Ce^{3+},Mn^{2+} Phosphors: A Facile Synthesis via the Soft-Chemical Ammonolysis Process, Luminescence, and Energy-Transfer Properties. *Inorg. Chem.* **2014**, *53*, 2230−2239.

(23) Van Uitert, L. G. An Empirical Relation Fitting the Position in Energy of the Lower D-band Edge for Eu^{2+} or Ce^{3+} in Various Compounds. *J. Lumin.* **1984**, *29*, 1−9.

(24) Zhai, D. Y.; Ning, L. X.; Huang, Y. C.; Liu, G. K. Ce−O Covalence in Silicate Oxyapatites and Its Influence on Luminescence Dynamics. *J. Phys. Chem. C* **2014**, *118*, 16051−16059.

(25) Xia, Z.; Wang, X.; Wang, Y.; Liao, L.; Jing, X. Synthesis, Structure, and Thermally Stable Luminescence of Eu^{2+}-Doped $Ba_2Ln(BO_3)_2Cl$ (Ln=Y, Gd and Lu) Host Compounds. *Inorg. Chem.* **2011**, *50*, 10134−10142.